J. CHEM. SOC. FARADAY TRANS., 1995, 91(22), 4161–4170

Surface Structure Change of a $[Pt_4(\mu\text{-}CH_3COO)_8]/SiO_2$ Catalyst Active for the Decomposition of Formic Acid

Wang-Jae Chun, Keiichi Tomishige,† Mamiko Hamakado and Yasuhiro Iwasawa*‡
Department of Chemistry, Graduate School of Science, The University of Tokyo, Hongo, Bunkyo-ku, Tokyo 113, Japan

Kiyotaka Asakura
Research Center for Spectrochemistry, Faculty of Science, The University of Tokyo, Hongo, Bunkyo-ku, Tokyo 113, Japan

Pt_4-cluster/SiO_2 catalyst, prepared from the $[Pt_4(\mu\text{-}CH_3COO)_8]$ cluster, has shown remarkably high catalytic activity with 100% selectivity to CO_2 and H_2 for the decomposition of formic acid as compared with the Pt-particle/SiO_2 catalyst. In order to elucidate the genesis and the mechanism for catalysis by Pt_4-cluster/SiO_2, the samples were characterized by kinetics, Pt L_{III}-edge extended X-ray absorption fine structure (EXAFS), and FTIR spectroscopy. EXAFS and IR data revealed that the surface structure of the catalyst changed from the tetramer to dimers during an induction period, then to monomers which were active for the catalysis. Eventually Pt particles were formed which were of much lower catalytic activity. The structural transformations of the Pt_4-cluster/SiO_2 catalyst are discussed in relation to the catalytic reaction profiles.

Knowledge of the structure and chemical state of the active site of a catalyst is indispensable to elucidate the catalytic reaction mechanism. New catalytic materials generate unique catalysis which may provide information on the genesis and the mechanism for efficient catalysis. At the surface of an inorganic oxide such as SiO_2 and Al_2O_3, novel metallic and metal-oxide species, which cannot be obtained in homogeneous solution systems, can be produced from organometallic and metal-cluster compounds, followed by chemical treatments when necessary.[1–3] The surface species obtained are often entirely different in nuclearities and structures, from those prepared by a traditional impregnation method using aqueous solution of metal salts.[1–5] One of the methods of supporting very small metal particles or clusters on oxide surfaces is the use of metal-cluster compounds as precursors, which are characterized by their unique framework consisting of three or more metal atoms and stabilized by appropriate ligands such as carbonyl, phosphines, halides, acetates, oxides, *etc.*[1–5] We found that the catalyst prepared by supporting $[Pt_4(\mu\text{-}CH_3COO)_8]$ on SiO_2 showed a remarkably high activity for formic acid decomposition compared with a Pt particle catalyst.

Decomposition of formic acid on metal and oxide surfaces has served as a convenient testing reaction for fundamental research in catalysis; *e.g.* to determine the factors which can affect the catalytic properties of metals and metal oxides.[6–11] It was also the first reaction which demonstrated that the catalytic performance of a metal was drastically influenced by the nature of the support.[12–15] There are also examples of studies of the mechanism of the catalytic decomposition of formic acid, such as the water-gas shift reaction (WGSR)[16–22] and the synthesis and decomposition of methanol.[23–27] Those examples indicate that the study of HCOOH decomposition is not only of academic interest, but also of strong relevance to some important industrial catalytic processes.

In the present study $[Pt_4(\mu\text{-}CH_3COO)_8]$[octakis($\mu$-acetato-*O,O′*) tetraplatinum(II)] was employed as a precursor for SiO_2-supported platinum catalyst, which is shown in Fig. 1.[28–30] The cluster has a square framework composed of four Pt atoms with strong metal–metal bonds at the distances 0.2493–0.2501 nm, and is coordinated by eight bridging acetate groups. Note that the Pt–Pt distance of the Pt_4-cluster is shorter than in other Pt clusters (0.258–0.265 nm) such as dimers[31,32] and trimers.[33,34] The arrangement of acetate ligands is such that four groups are approximately in the cluster plane, while four others are alternately above and below it. The molecular structure is similar to that for the tetragonal form, but shows a twisting distortion away from ideal $42m(D_{2d})$ symmetry. Yamaguchi *et al.* reported facile regioselective ligand substitution for the in-plane bridging acetate in the Pt cluster.[35,36] They observed that only in-plane acetate groups were easily replaced by carboxylic acids (RCOOH; R = CH_3, CCl_3, CF_3, C_6H_5) in solution, then the structure was changed to $[Pt_4(\mu\text{-}CH_3COO)_4(\mu\text{-}HCOO)_4]$. From those properties, we could expect that the catalyst employing the cluster would exhibit unique catalytic properties for formic acid decomposition (R = H) because decomposition of the formate intermediate in the WGRS was remarkably promoted by co-adsorbates, showing a drastic change of the selectivity.[18–22] Thus, we studied the performance of the catalyst prepared from $[Pt_4(\mu\text{-}CH_3COO)_8]$ on silica support for decomposition of formic acid.

The aim of this study is to examine the catalytic properties of the Pt_4-cluster/SiO_2 catalyst, to reveal the structure of the active species by EXAFS and FTIR spectroscopy, and to discuss the reaction mechanism.

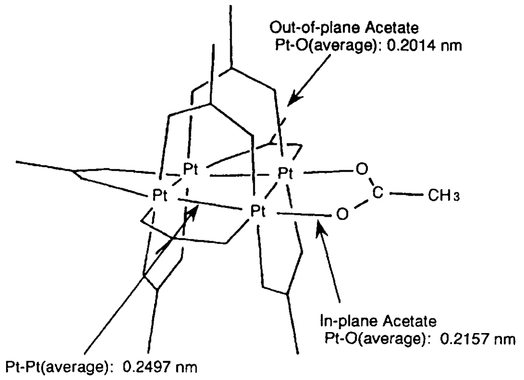

Fig. 1 Structure of $[Pt_4(\mu\text{-}CH_3COO)_8]$

---

† Present address: Department of Applied Chemistry, Faculty of Engineering.

‡ Electronic mail: iwasawa@utsc.s.u-tokyo.ac.jp

Experimental

Preparation of Pt_4-cluster/SiO_2 catalyst

The cluster $[Pt_4(\mu\text{-}CH_3COO)_8]$ was prepared using the method of Yamaguchi *et al.*, and was characterized with ^1H NMR.[35,36] SiO_2 (Fuji-Davison Silicagel no. 952, surface area: 300 m^2 g^{-1}), was calcined at 573 K for 1 h in air, followed by evacuation. The cluster was dissolved in CH_2Cl_2, and impregnated on the pretreated SiO_2 for 1 h, followed by evacuation to remove the solvents. All procedures of preparation of the catalyst except for the calcination of SiO_2 were carried out in a vacuum line or under an Ar atmosphere. The Pt content of the catalysts was 1.0 wt.%.

Preparation of Pt-particle/SiO_2 catalyst

A 1.0 wt.% Pt/SiO_2 catalyst was prepared by an ion-exchange method. SiO_2 was stirred overnight in an excess of aqueous ammonium hydroxide. The preparation was followed by adding $Pt(NH_3)_4Cl_2 \cdot H_2O$ dissolved in distilled water to the ion-exchange system. The solution was stirred overnight. The sample was then filtered, washed with distilled water, then dried at 343 K. The catalyst was calcined at 573 K for 1 h, followed by reduction with H_2 at 473 K for 1 h.

Decomposition of formic acid on the Pt_4-cluster/SiO_2 catalyst

The catalytic decomposition of formic acid was carried out in a closed circulating system equipped with a gas chromatograph. 5A molecular sieve and Porapak PS columns were used for the analysis of reactant and products. A quadrupole mass spectrometer (AQA-100R, ANELVA) was also employed to analyse the products. Research-grade formic acid was purified over $MgSO_4$, followed by distillation. The pressure of formic acid was maintained at 1.47 kPa during the catalytic reaction. In the study on the induction period, 0.07 kPa of the initial pressure of formic acid was introduced into the system. Isotope effects were examined with DCOOH, DCOOD and HCOOD (purchased from Cambridge Isotope Laboratories). These were used without further purification. The composition for the isotopes are listed as follows; DCOOH(D: 89%), DCOOD(D: 89%) and HCOOD(D: 89%).

Characterization by ^1H NMR

^1H NMR spectra were recorded on a Hitachi R-24B using $CDCl_3$ as the solvent.

Characterization by FTIR Spectroscopy

IR spectra of the catalyst in the course of formic acid decomposition were recorded with a Jasco FT/IR-7000 Spectrometer using a liquid-nitrogen-cooled MCT detector. The measurements were conducted at room temperature and over 100-200 scans at a resolution of 2 cm^{-1}. The IR cell used in this study was made from Pyrex glass and has a pair of NaCl windows, which were cooled with circulating water to avoid the damage to the windows during heat treatments of the catalyst. The cell was combined with a closed circulating system. A self-supporting disc of SiO_2 powder (50 mg) mounted in the IR cell was calcined at 573 K, similarly to the catalyst preparation. The spectrum of the treated SiO_2 was recorded after cooling to room temperature. $[Pt_4(\mu\text{-}CH_3COO)_8]/SiO_2$ was prepared by impregnating the SiO_2 disc with a solution of $[Pt_4(\mu\text{-}CH_3COO)_8]$ in CH_2Cl_2 by using a capillary under an Ar atmosphere in the IR cell. Then the remaining solvent was removed by evacuation. The IR spectrum was recorded with the fresh sample. The spectra during the formic acid decomposition reactions under various conditions were taken successively as a function of reaction time. All the spectra shown in this paper were background subtracted.

Characterization by *in situ* EXAFS

X-ray absorption fine structure spectra at the Pt L_{III}-edge were measured on beam line BL10B of the National Laboratory for High Energy Physics (KEK-PF). The storage ring operated at an electron energy of 2.5 GeV with the beam current 250–350 mA. An Si(311) channel-cut crystal monochromator was used to produce monochromatic X-rays from the synchrotron radiation, since this monochromator produces almost no second-order harmonics. X-Ray absorption data were collected in transmission mode using two ionization chambers filled with N_2 (I_0) and N_2 (85%)–Ar (15%) (I) as X-ray detectors. Samples for the EXAFS measurement were prepared and treated in the same way as the samples used for the catalytic reaction in a closed-circulating system and were transferred without contacting air to glass cells equipped with Kapton windows for the EXAFS measurement. The cell for the Pt L_{III}-edge EXAFS measurement was 10 mm thick which allows enough edge height for total absorbance $\mu x = 1\text{–}2$. The sample in the sealed glass cell was kept in a container at 195 K until the measurement, which was performed at 70 K and at room temperature. Data were analysed using the program EXAFS2.[37] The analysis involved pre-edge extrapolation, background removal by a cubic spline method to extract EXAFS data, and Fourier transformation using a Hanning window function using one-tenth of the FT range. The typical ranges of Fourier transformation from k space to r space were 30–150 nm^{-1} for the Pt L_{III} edge. The inverse Fourier transformation to k space and the curve fitting were carried out to obtain detailed structural information. Empirical parameters extracted from Pt foil and $(NH_4)_4[H_4PtMo_6O_{24}]$ for Pt—O bond were used as references to analyse Pt—Pt and Pt—O bonds, respectively.[38] The coordination number in this report was corrected for the R dependence of the EXAFS amplitude by the equation,[39]

$$N = N^* \exp[2(R - R_s)/\lambda]$$

where N is the corrected coordination number and N^* is the coordination number determined from the analysis. R_s is the interatomic distance found from the analysis of the sample, R is the crystallographic distance of the reference sample and λ is the mean free path (1 nm). The accuracy of the values from the analysis is reported to be better than 0.02 nm for distance and *ca.* 10% for coordination number.[40] The validity of the curve fitting was judged not only from ΔE_0 and the Debye-Waller factor, σ, but also from the R factor (R_f)

$$R_f = \int_{k_{min}}^{k_{max}} |k^3\chi^{obs}(k) - k^3\chi^{calc}(k)|^2\, dk \Big/ \int_{k_{min}}^{k_{max}} |k^3\chi^{obs}(k)|^2\, dk$$

Results and Discussion

Characterization of the Pt_4-cluster/SiO_2 catalyst

In order to investigate the structure of the catalyst, we performed the EXAFS analysis which was compared with the unsupported cluster. The k^3-weighted Fourier transformation of the EXAFS data for $[Pt_4(\mu\text{-}CH_3COO)_8]$/BN and the supported cluster was achieved over the range $30 < (k/nm^{-1}) < 150$. The range of the inverse Fourier transform-

Table 1 Curve fitting results of Pt L_{III}-edge spectra for $[Pt_4(\mu\text{-}CH_3COO)_8]$/BN (1) and $[Pt_4(\mu\text{-}CH_3COO)_8]/SiO_2$ (2)

sample	bond	CN	R/nm	ΔE_0/eV[a]	σ/nm	R_f (%)
(1)	Pt—O	2.0	0.201	−3.5	0.0056	2.2
	Pt—O	2.0	0.217	−3.5	0.0075	
	Pt—Pt	2.0	0.251	−0.5	0.0048	
(2)	Pt—O	2.3	0.201	− 3.5	0.0060	2.6
	Pt—O	1.9	0.217	−3.5	0.0080	
	Pt—Pt	2.0	0.251	− 0.5	0.0055	

[a] Difference between origins of the photoelectron wavevector.

ation was $0.14 < (R/\text{nm}) < 0.29$. EXAFS spectra, Fourier transformation and curve fitting for the precursor are shown in Fig. 2(*a*). The first shell (0.14–0.20 nm) in the Fourier transformation is assigned to Pt—O bond and the second shell (0.20–0.29 nm) is assigned to Pt—Pt bond. Based on the crystallographic structure of the precursor, we performed three-wave (Pt—O + Pt—O + Pt—Pt) curve fitting as shown in Fig. 2 (a-3). In the present analysis the number of independent parameters ($N_1 = 2\Delta k\, \Delta R/\pi + 2$) is 13.5, which would also make the three-wave analysis valid.[41] However, the curve fitting analysis was conducted by fixing the coordination numbers (CN) to give the best agreement with the crystallographic data as shown in Table 1.[28–30] The results for the Pt_4-cluster/SiO_2 catalyst are presented in Fig. 2(*b*) and Table 1. There was difference between spectra for $[Pt_4(\mu\text{-}CH_3COO)_8]$ and Pt_4-cluster/SiO_2 samples. The best fit result for the catalyst in Table 1 was obtained by changing the parameters, CN, R and σ, while ΔE_0 was fixed to the same values as those for the precursor. The structural data for the catalyst are almost the same as those for the precursor itself.

To confirm the results of the EXAFS analysis the IR spectra of both $[Pt_4(\mu\text{-}CH_3COO)_8]/CDCl_3$ and $[Pt_4(\mu\text{-}CH_3COO)_8]/SiO_2$ systems were measured. The peaks at 1565, 1438, 1414, 1457 and 1347 cm^{-1} for the acetate ligands of the cluster in $CDCl_3$ are straightforwardly assigned to $\nu_a(OCO)$, $\nu_s(OCO)$(out-of-plane); $\nu_s(OCO)$(in-plane), $\delta_a(CH_3)$ and $\delta_s(CH_3)$, respectively,[42,43] as listed in Table 2. The $[Pt_4(\mu\text{-}CH_3COO)_8]/SiO_2$ catalyst showed almost the same spectra at 1564, 1442, 1418, 1462 and 1350 cm^{-1} for the above assigned bands, respectively.

Accordingly, the EXAFS and IR data conclude that the framework of the cluster is maintained when supported on SiO_2.

Catalytic Decomposition of Formic Acid

The profile of the catalytic decomposition of formic acid HCOOH on the $[Pt_4(\mu\text{-}CH_3COO)_8]/SiO_2$ catalyst is shown in Fig. 3. There was an induction period of *ca.* 10 min for the reaction, during which time no product was observed in the

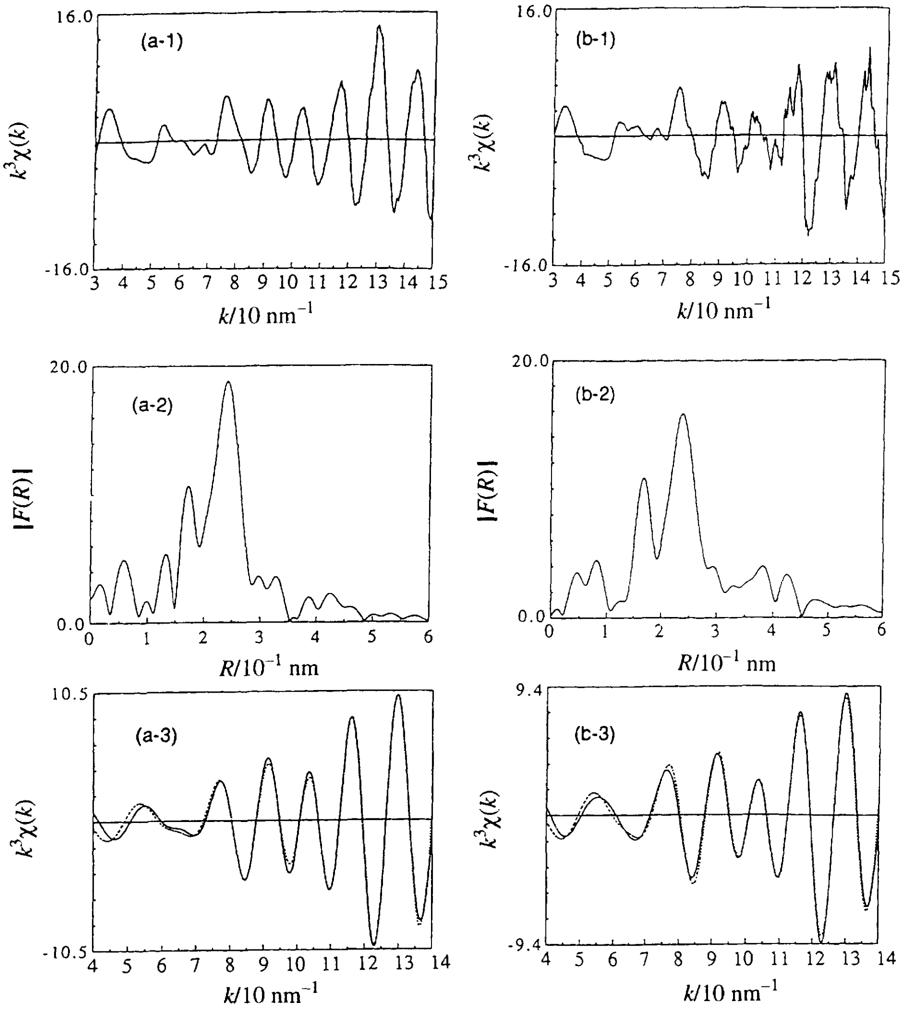

Fig. 2 EXAFS spectra for (a) $[Pt_4(\mu\text{-}CH_3COO)_8]$/BN and (b) $[Pt_4(\mu\text{-}CH_3COO)_8]/SiO_2$ measured at 70 K; (1) k^3-weighted EXAFS oscillation; (2) Fourier transformation (k = 30–150 nm^{-1}); (3) curve fitting (R = 0.14–0.29 nm) (Pt—O, Pt—O and Pt—Pt). Solid line: observed; broken line: calculated.

Table 2 IR peaks (cm^{-1}) of the bridging acetates for $[Pt_4(\mu\text{-}CH_3COO)_8]/CDCl_3$ (1) and $[Pt_4(\mu\text{-}CH_3COO)_8]/SiO_2$ (2)

assignment	(1)	(2)
$\nu_a(OCO)$	1565	1564
$\nu_s(OCO)^a$	1438	1442
$\nu_s(OCO)^b$	1414	1418
$\delta_a(CH_3)$	1457	1462
$\delta_s(CH_3)$	1347	1350

[a] Out-of-plane acetate. [b] In-plane acetate.

gas phase. The reaction of HCOOH (constant pressure of 1.47 kPa at 288 K) then began and the catalytic decomposition of HCOOH was found to be remarkably promoted at *ca.* 18 min, then a steady-state reaction proceeded as shown in Fig. 3. In the steady-state, equal amounts of CO_2 and H_2 were produced in a closed circulation system (Fig. 3). The catalytic reaction rates in the steady-state [turnover frequency (TF): CO_2 molecules produced per min per Pt atom] were plotted *vs.* the reciprocal reaction temperature in Fig. 4, which gave an activation energy of 69 kJ mol^{-1}. The selectivity toward $CO_2 + H_2$ (dehydrogenation) was 100%. On the other hand, the catalytic decomposition of formic acid on the Pt-particle/SiO_2 catalyst under identical conditions was negligible (two–three orders of magnitude less than the activity for the Pt_4-cluster/SiO_2 catalyst). In Fig. 4 the Arrhenius plots for the dehydrogenation and dehydration reactions of HCOOH are also shown over a much higher temperature range. Both combinations, $CO_2 + H_2$ and $CO + H_2O$, were produced, which is in contrast with the case of the Pt_4-cluster/SiO_2 catalyst. The activation energies for the dehydrogenation and the dehydration were calculated to be 41 and 73 kJ mol^{-1}, respectively. The remarkably high catalytic activity of the Pt_4-cluster/SiO_2 catalyst almost ceased to exist eventually after 60 min reaction as shown in Fig. 3.

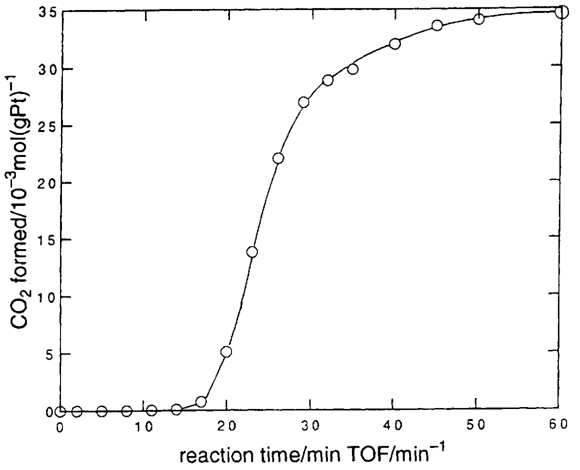

Fig. 3 Profile of the catalytic decomposition reaction of formic acid (1.47 kPa) on $[Pt_4(\mu\text{-}CH_3COO)_8]/SiO_2$ at 288 K

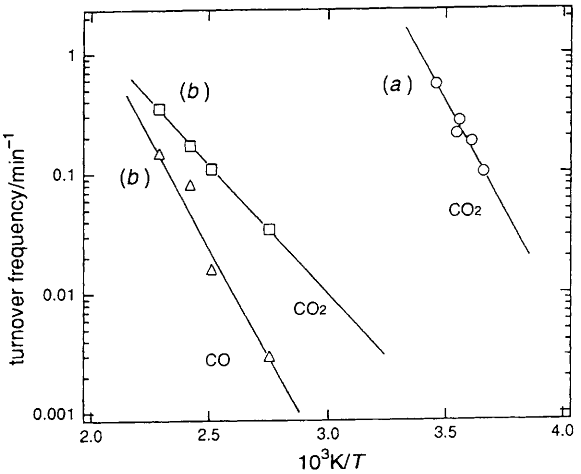

Fig. 4 Arrhenius plots for the catalytic decomposition reactions of formic acid on $[Pt_4(\mu\text{-}CH_3COO)_8]/SiO_2$ (*a*) and ion-exchanged Pt/SiO_2 (*b*)

The detailed profile of the decomposition reactions of HCOOH, DCOOH and DCOOD is shown in Fig. 5 in order to understand the genesis of the highly active catalysis of the supported clusters and to trace the behaviour and mechanism of the reaction. A common feature with formic acid and deuterium-labelled formic acid, is that there is an induction period for the first 10–14 min, followed by a slow reaction step prior to the high-rate reaction (Fig. 5). The reaction rates (TF) for HCOOH, DCOOH and DCOOD in the slow reaction step were 0.0059, 0.0025 and 0.0017 min^{-1}, respectively, showing isotope effects for both C—H and O—H bonds of formic acid molecule. Isotope effects were also observed in the high-rate reaction step as shown in Fig. 6; the activation energies for the decomposition reactions of HCOOH, HCOOD, DCOOH and DCOOD were 69, 54, 49 and 24 kJ mol^{-1}, respectively. From those results, we presume that the formic acid decomposition reaction is accompanied with an induction period, a slow reaction step, a high-rate reaction step, and a deactivation process.

Characterization of the Surface Pt Sites

1. Preceding Induction Period

IR spectra were measured to investigate what kind of structural change occurred in the induction step. Since HCOOH reacted too fast to observe easily, we employed DCOOD as the reactant to follow the behaviour of surface active species. Fig. 7 shows the IR spectra recorded at intervals in the decomposition reaction of DCOOD at 305 K on the $[Pt_4(\mu\text{-}CH_3COO)_8]/SiO_2$ catalyst disc. The peak at 1418 cm^{-1} for the in-plane acetate ligands was replaced by the in-plane formate ligands characterized by the 1304 cm^{-1} peak,

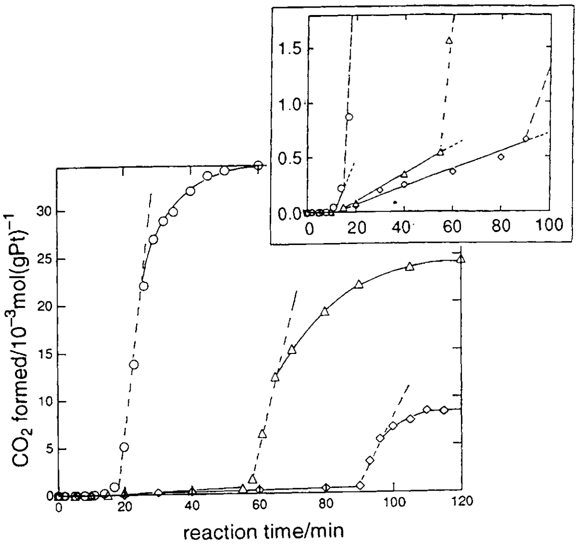

Fig. 5 Profiles of the decomposition reactions of HCOOH (○), DCOOH (△) and DCOOD (◇) at 288 K. HCOOH: 1.47 kPa; DCOOH: 1.07 kPa; DCOOD: 1.47 kPa (constant pressure). Gradients: (– – –, main figure) 0.5401 (○), 0.234 (△) and 0.146 min^{-1} (◇); (——, insert) 0.0059 (○), 0.0025 (△) and 0.0017 min^{-1} (◇).

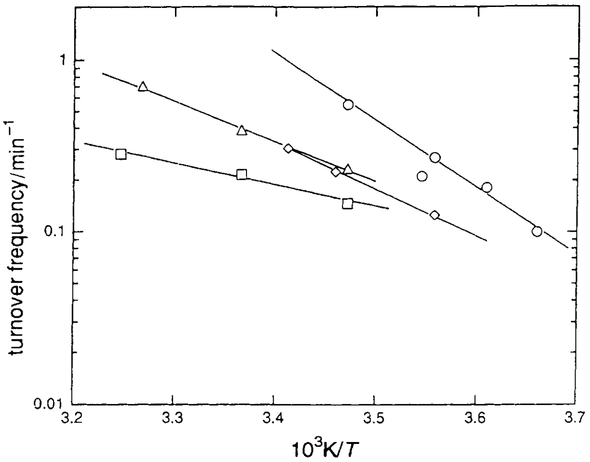

Fig. 6 Arrhenius plots for the decomposition reactions of HCOOH (○), DCOOH (△), HCOOD (◇) and DCOOD (□) with gradients of 69, 49, 54 and 24 kJ mol^{-1}, respectively

whereas the out-of-plane acetates were not replaced by formic acid, as proved by no change of the peak at 1442 cm^{-1}. This preferential replacement of the in-plane acetates was also observed in a $CDCl_3$ solution of $[Pt_4(\mu\text{-}CH_3COO)_8]$ and was also confirmed by ^1H NMR which revealed ready exchange of the in-plane acetates (2.40 ppm) with formic acid in $CDCl_3$ which was completed within 2 min at room temperature, whereas the intensity of the peak (1.98 ppm) for the out-of-plane acetates remained almost unchanged. The exchange reaction favourable at the in-plane sites agrees with the results in the literature for organic carboxylates.[44] Thus it may be concluded that the cluster $[Pt_4(\mu\text{-}CH_3COO)_8]$ on SiO_2 is converted to $[Pt_4(\mu\text{-}CH_3COO)_4(\mu\text{-}HCOO)_4]/SiO_2$ by exposing the cluster to HCOOH vapour. After the replacement of four in-plane acetates in $[Pt_4(\mu\text{-}CH_3COO)_8]/SiO_2$ by formates within 2 min, no further significant change in the IR spectrum was observed in the induction period [Fig. 7(*b*) and (*c*)].

To characterize the structure of the cluster $[Pt_4(\mu\text{-}CH_3COO)_4(\mu\text{-}HCOO)_4]$ on SiO_2, we performed the EXAFS analysis for this cluster. Fig. 8 shows the EXAFS oscillation in the range $30 \leqslant (k/\text{nm}^{-1}) \leqslant 150$, its associated Fourier transformation and the curve fitting [inverse Fourier transform range, $0.14 \leqslant (R/\text{nm}) \leqslant 0.29$]. Comparing with the EXAFS spectra of the $[Pt_4(\mu\text{-}CH_3COO)_8]/SiO_2$ catalyst, there is no sign of change in the cluster structure, except slight depression around 0.16 nm in the Fourier transformation which can be referred to the replacement of in-plane acetates by formates. The curve fitting analysis was conducted in a similar way to that for the $[Pt_4(\mu\text{-}CH_3COO)_8]/SiO_2$ catalyst. The best-fit result for $[Pt_4(\mu\text{-}$

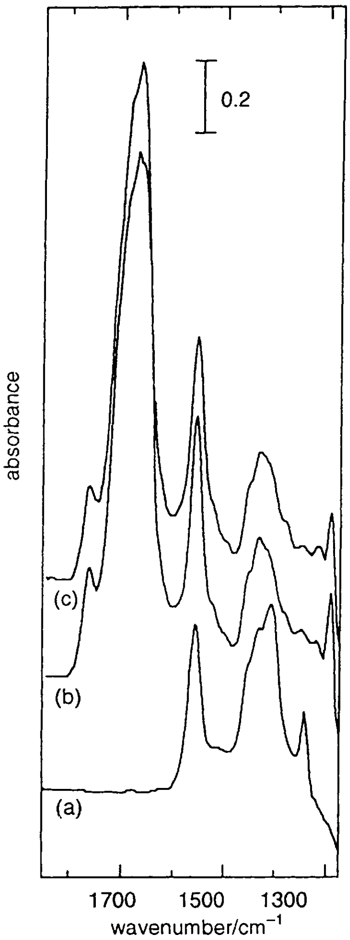

Fig. 7 IR spectra for $[Pt_4(\mu\text{-}CH_3COO)_8]/SiO_2$ in the induction period of DCOOD reaction at 305 K: (a) 0, (b) 2 and (c) 8 min

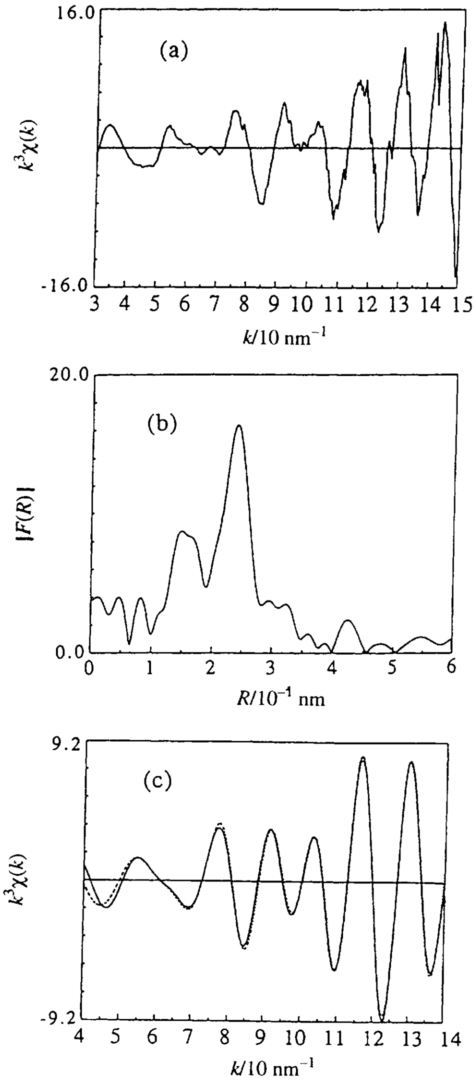

Fig. 8 EXAFS data for $[Pt_4(\mu\text{-}CH_3COO)_8]/SiO_2$ in the induction period of the HCOOH reaction at 289 K; measured at 110 K; (a) k^3-weighted EXAFS oscillation; (b) Fourier transformation (k = 30–150 nm^{-1}); (c) curve fitting (R = 0.14–0.29 nm) (Pt—O, Pt—O and Pt—Pt). Solid line: observed; broken line: calculated.

Table 3 Three-wave curve fitting result of Pt L_{III}-edge spectra for the catalyst during the induction period

bond	CN	R/nm	ΔE_0/eV	σ/nm	R_f (%)
Pt—O	2.4	0.198	−3.5	0.0058	2.1
Pt—O	2.4	0.217	−3.5	0.0070	
Pt—Pt	2.0	0.251	−0.5	0.0050	

$CH_3COO)_4(\mu$-$HCOO)_4]/SiO_2$ is shown in Fig. 8(*c*) and Table 3. There was no significant difference in the structural parameters determined by EXAFS between $[Pt_4(\mu$-$CH_3COO)_8]/SiO_2$ and $[Pt_4(\mu$-$CH_3COO)_4(\mu$-$HCOO)_4]/SiO_2$ (Tables 1 and 3).

Accordingly, IR and EXAFS data revealed that $[Pt_4(\mu$-$CH_3COO)_8]$ on SiO_2 was transformed to $[Pt_4(\mu$-$CH_3COO)_4(\mu$-$HCOO)_4]$ without change of the cluster framework in the induction period.

2. Slow Reaction Step

We assume this step as a transformation stage for the cluster structure because the cluster framework did not change during the preceding induction period, while in the subsequent period the decomposition of formic acid gradually proceeded. Under the catalytic reaction conditions at saturation of adsorbed formic acid, it is impossible to characterize the structure of the active sites formed because the next step is too rapid in the presence of gas-phase formic acid. Therefore, we adopted a different reaction condition for the study of the step by introducing a low pressure of formic acid (0.07 kPa). The amount of introduced formic acid is more than the in-plane acetate sites in the catalyst employed, but there is no more in the gas phase during the reaction. The reaction proceeded gradually and stopped after 180 and 420 min for HCOOH and DCOOH, respectively as shown in Fig. 9. The total amount of CO_2 produced in the low-pressure reactions was the same with both HCOOH and DCOOH, although the reaction rates were different. The total amount of CO_2 was also almost the same as the expected value produced by the decomposition of the replaced in-plane formate ligands. After the decomposition reaction was complete, HCOOH or DCOOD of 1.47 kPa was admitted to the system. The reaction began again, showing similar high reaction rates to those in the catalytic reaction conditions of Fig. 5. Thus, the state at which the low-pressure reaction stopped may be an active intermediate species on which the high-rate reaction is induced.

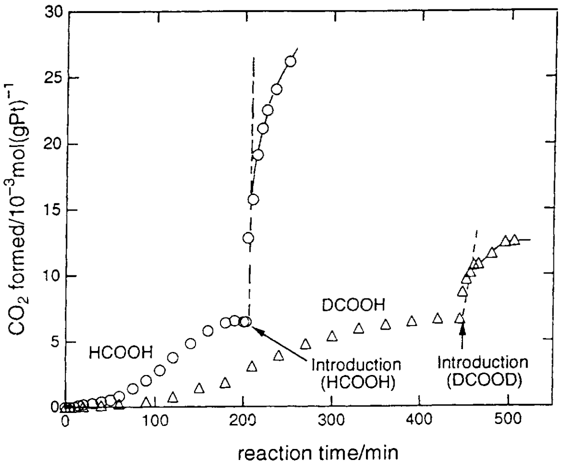

Fig. 9 Profiles of the decomposition reactions of HCOOH (○) or DCOOH (△) at an initial pressure of 0.07 kPa, followed by introduction of 1.47 kPa of HCOOH or DCOOD at 288 K. Gradients: (---) 0.52 (○) and 0.14 min^{-1} (△).

To obtain information on the active intermediate platinum species, IR spectra (Fig. 10) for the slow step were taken under identical conditions to the reaction. The 1418 cm^{-1} peak for the in-plane acetates was replaced by a peak at 1302 cm^{-1} for the in-plane formate (DCOO), where the 1418 cm^{-1} peak did not completely diminish. The peak of 1302 cm^{-1} decreased gradually and disappeared completely by the decomposition reaction. The decreasing rate of the formate ligands in the IR spectra coincided well with the rate of CO_2 formation. Thus, the CO_2 formation observed in the slow reaction period is suggested to be due to the decomposition of the in-plane formate ligands in the $[Pt_4(\mu$-$CH_3COO)_4(\mu$-$HCOO)_4]$ on SiO_2. Acetate ligands were found on Pt species at the end of the slow decomposition reaction, as shown in Fig. 10. The number of acetate ligands coordinated to Pt atoms was estimated to be approximately an acetate ligand per Pt atom from comparison of the intensity of the IR peaks for the surface species at the end of the slow reaction with that of the IR peaks for the incipient Pt species $[Pt_4(\mu$-$CH_3COO)_8]/SiO_2$.

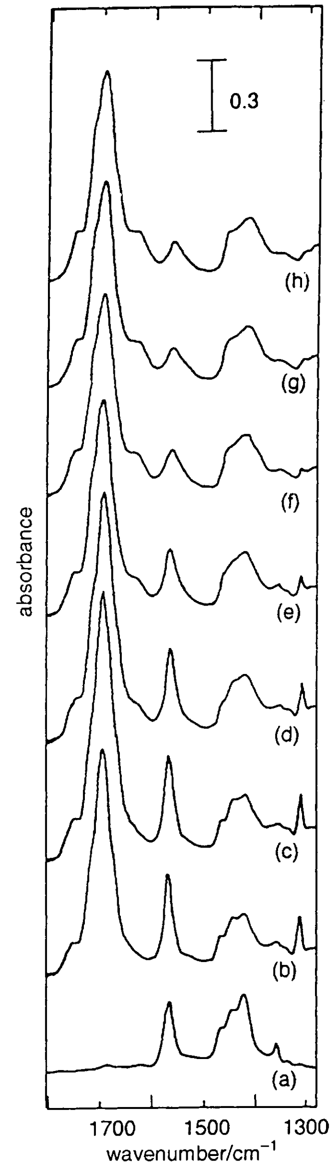

Fig. 10 IR spectra for $[Pt_4(\mu$-$CH_3COO)_8]/SiO_2$ in the slow reaction period at 303 K with 0.07 kPa of DCOOH: (a) 0, (b) 2, (c) 15, (d) 60, (e) 120, (f) 240, (g) 360 and (h) 420 min

In order to determine the structure of the Pt species formed in the slow decomposition step, we performed an EXAFS analysis for the sample at the end of the slow reaction (at 180 min in Fig. 9). The Pt L_{III}-edge EXAFS data are presented in Fig. 11. The oscillation [Fig. 11(*a*)] and Fourier transform [Fig. 11(b)] are entirely different from those for $[Pt_4(\mu\text{-}CH_3COO)_8]$ itself [Fig. 2(*a*)], $[Pt_4(\mu\text{-}CH_3COO)_8]/SiO_2$ [Fig. 2(*b*)] and the sample during the induction period (Fig. 8), which suggests a partial decomposition of the original cluster framework at this reaction stage. The best-fit for the inversely Fourier-transformed oscillation was carried out in Fig. 11(*c*) and the determined bond distances and coordination numbers for Pt—O, Pt—O and Pt—Pt bonds are listed in Table 4, which indicates the existence of a Pt—Pt bond and two different Pt—O bonds.

From the IR and EXAFS results, we suspect that the shorter Pt—O bonds at 0.203 nm are related to the remaining acetate ligands, where the acetate : Pt ratio is 1 suggested by the IR data is compatible with the coordination number (2.1) for the Pt—O bond only if the Pt species is a dimer. The Pt—Pt bond at 0.250 nm exhibits a coordination number of 1.2, which may confirm a dimeric structure, comparing the coordination numbers of 2.0 for the Pt_4 tetramers in Tables 1 and 3. Then, the longer Pt—O bond at 0.220 nm (CN = 1.5) may be assigned to the bonding of a Pt atom with an oxygen atom at the SiO_2 surface. We think that the in-plane formate ligands were decomposed to CO_2 and H_2, accompanied by the reaction of the resultant coordinately unsaturated Pt atoms with the surface OH groups. The participation of the surface OH groups in the decomposition of the in-plane formates during the slow-reaction period at an initial pressure of formic acid of 0.07 kPa was suggested by the isotope effects observed in Fig. 5. When DCOOD was used as a reactant, the surface OH groups were converted to the OD groups immediately after the introduction of DCOOD to the system as proved by IR, while the OH groups were not transformed to the OD groups by DCOOH. In both cases the same peak for the in-plane DCOO ligands was observed. Therefore, the difference of the isotope effect between DCOOH and DCOOD during the slow reaction period is referred to the contribution of the surface OH groups to the in-plane formate decomposition at least in the absence of gas-phase formic acid. The ratio of CO_2 to H_2 produced by the in-plane formate decomposition in the slow process is 1 : 0.8, which is close to 1 : 1, considering the experimental error in a mass-spectrometric quantification. If the in-plane formate ligands decomposed by themselves, the ratio of CO_2 to H_2 would be 1 : 0.5 and almost no isotope effect would be observed with the OH hydrogen.

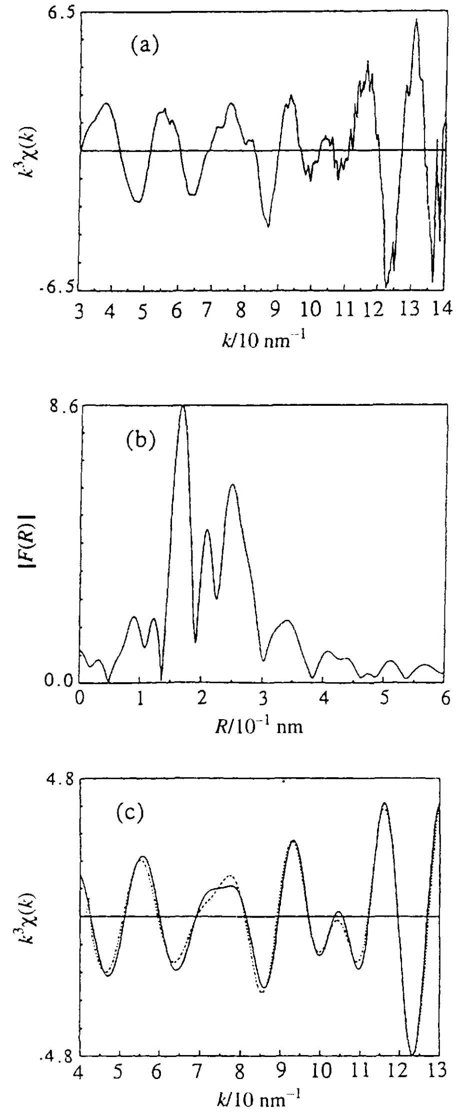

Fig. 11 EXAFS data for $[Pt_4(\mu\text{-}CH_3COO)_8]/SiO_2$ at the end of the slow reaction period at 288 K with 0.07 kPa of HCOOH after 180 min; measured at 70 K; (a) k^3-weighted EXAFS oscillation; (b) Fourier transformation (k = 30–140 nm^{-1}); (c) curve fitting (R = 0.14–0.30 nm) (Pt—O, Pt—O and Pt—Pt). Solid line: observed; broken line: calculated.

Table 4 Three-wave curve fitting result of Pt L_{III}-edge spectra for the catalyst at the end of the slow reaction period

bond	CN	R/nm	ΔE_0/eV	σ/nm	R_f (%)
Pt—O	2.1	0.203	2.0	0.0050	3.4
Pt—O	1.5	0.220	2.5	0.0040	
Pt—Pt	1.2	0.250	2.0	0.0050	

3. Catalytic High-rate Reaction

IR spectra in the catalytic high-rate reaction region exhibited no peak for acetate ligands, when only physisorbed formic acid was observed at 1689 and 1388 cm^{-1} for ν(C=O) and ν_s(OCO), respectively. Thus, it is likely that the dimeric Pt structure as an active intermediate species was further converted to another species which is catalytically active.

The sample for the EXAFS measurement was prepared as follows. The $[Pt_4(\mu\text{-}CH_3COO)_8]/SiO_2$ catalyst was exposed to a constant pressure (1.47 kPa) of formic acid, then was monitored by a mass spectrometer for the formation of CO_2 and H_2. Immediately after the reaction attained the steady-state rate, the sample was cooled to a liquid-nitrogen temperature during evacuation followed by transfer of the sample to an EXAFS cell which was kept in a container at 195 K until the EXAFS measurement. The Pt L_{III}-edge k^3-weighted EXAFS oscillation, its associated Fourier transformation and the curve-fitting analysis are shown in Fig. 12. Initially we tried to fit a peak at 0.23 nm (phase shift uncorrected) in the Fourier transform by assuming it to be due to Pt—Pt bonding, but a satisfactory fit was never achieved. On the other hand, a peak at 0.17 nm was straightforwardly assigned to Pt—O bonding. Next, we performed the curve-fitting analysis over a whole range (0.11–0.27 nm) by assuming the first and second peaks in the Fourier transform as Pt—O bonds. The results are shown in Fig. 12(*c*) and in Table 5, where two different Pt—O bonds at 0.201 and 0.266 nm were discriminated, reflecting the two separated peaks in the Fourier transformation [Fig. 12(b)]. From these results we can conclude that the catalytically active species is a Pt monomer. We also propose a unique Pt monomeric structure

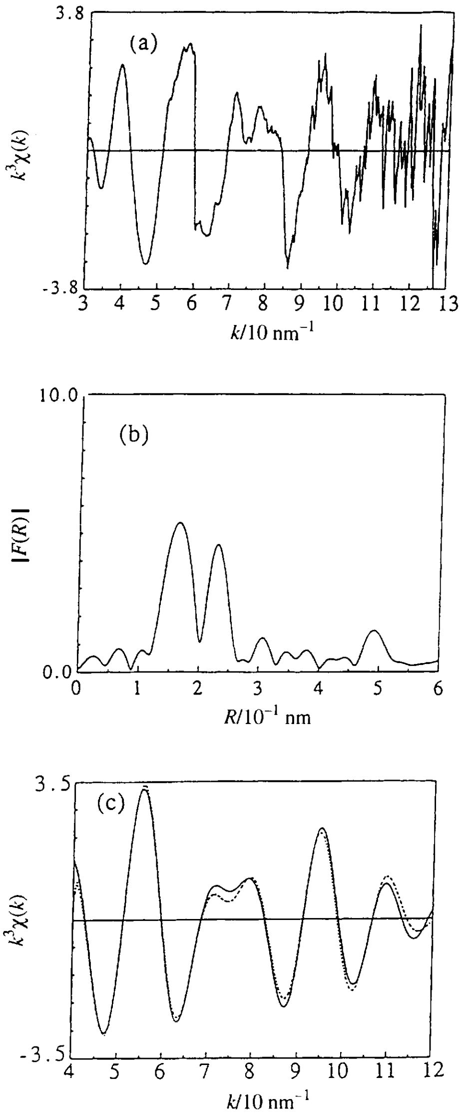

Fig. 12 EXAFS data for the catalyst in the catalytic reaction region; HCOOH: 1.47 kPa at 284 K; measured at 70 K; (a) k^3-weighted EXAFS oscillation; (b) Fourier transformation (k = 30–130 nm^{-1}); (c) curve fitting (R = 0.11–0.27 nm) (Pt—O + Pt—O). Solid line: observed, broken line: calculated.

which has 2–3 long Pt—O bonds at 0.266 nm besides two usual Pt—O bonds at 0.201 nm as illustrated in Scheme 1. Similar observation of long Pt—O bonds has been reported in the literature.[45] In regard to the oxidation state of Pt monomers, it is likely that the Pt atoms are dispersed in the oxidized state close to a bivalent state, judging from the peak intensity of the white line at the Pt L_{III}-edge compared with those for [$Pt_4(\mu\text{-}CH_3COO)_8$]/BN,[$Pt_4(\mu\text{-}CH_3COO)_8$]/$SiO_2$ and Pt metal.

4. Deactivation Process

After the catalytic decomposition of formic acid proceeded at the high reaction rate, eventually the catalyst was deactivated as shown in Fig. 3 and 5. To examine the deactivation process the EXAFS spectra for the almost deactivated catalyst were recorded in a similar manner to the others. Comparing the EXAFS spectra of this sample with those for the Pt_4-cluster and the supported Pt_4-cluster catalysts in the induction period, in the slow reaction region, and in the high-rate reaction region, it is obvious that a drastic change in the Pt structure has occurred. That is, the oscillation and Fourier transform in Fig. 13 are similar to those for Pt foil, which demonstrates that the Pt monomers aggregated to Pt particles under formic acid decomposition reaction conditions which are reducible atmosphere. In fact, the k-space oscillation was well reproduced by Pt—Pt bonding as shown in Fig. 13(*c*). The bond distance and coordination number for Pt—Pt were determined to be 0.276 nm and 6.6, respectively, in Table 6. We estimate the Pt particles to be *ca.* 0.9 nm in diameter, assuming a spherical shape.[46] A particle is equivalent to approximately five Pt_4-clusters. Thus, the aggregation to form particles is concluded to be the deactivating factor.

Table 5 Two-wave curve fitting result of Pt L_{III}-edge spectra for the catalyst during the catalytic reaction

bond	CN	R/nm	ΔE_0/eV	σ/nm	R_f (%)
Pt—O	2.2	0.201	−1.6	0.0056	3.4
Pt—O	2.6	0.266	1.8	0.0075	

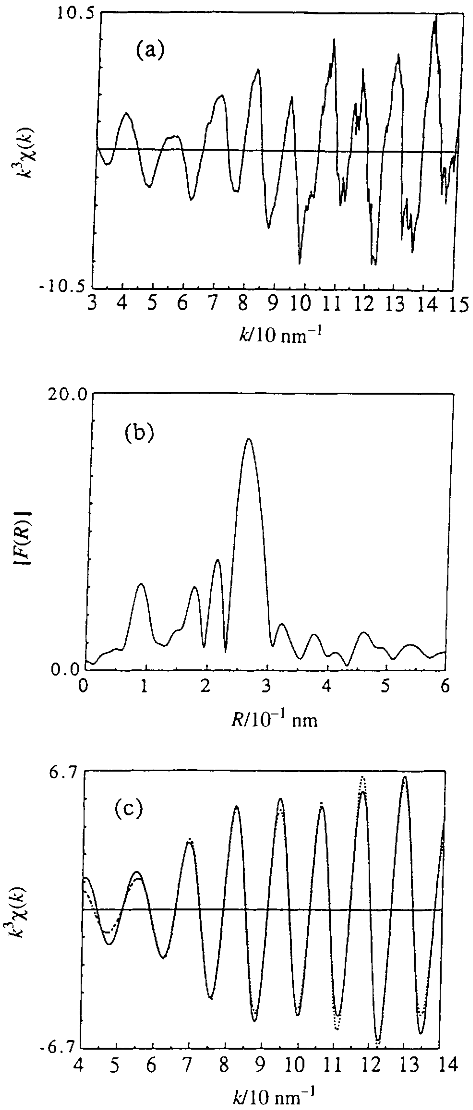

Fig. 13 EXAFS data for the deactivated catalyst measured at 70 K; (a) k^3-weighted EXAFS oscillation; (b) Fourier transformation (k = 30–150 nm^{-1}); (c) curve fitting (R = 0.18–0.31 nm) (Pt—Pt). Solid line: observed, broken line: calculated.

Table 6 One-wave curve fitting result of Pt L_{III}-edge spectra for the deactivated catalyst

bond	CN	R/nm	ΔE_0/eV	σ/nm	R_f (%)
Pt—Pt	6.6	0.276	−2.3	0.0081	3.3

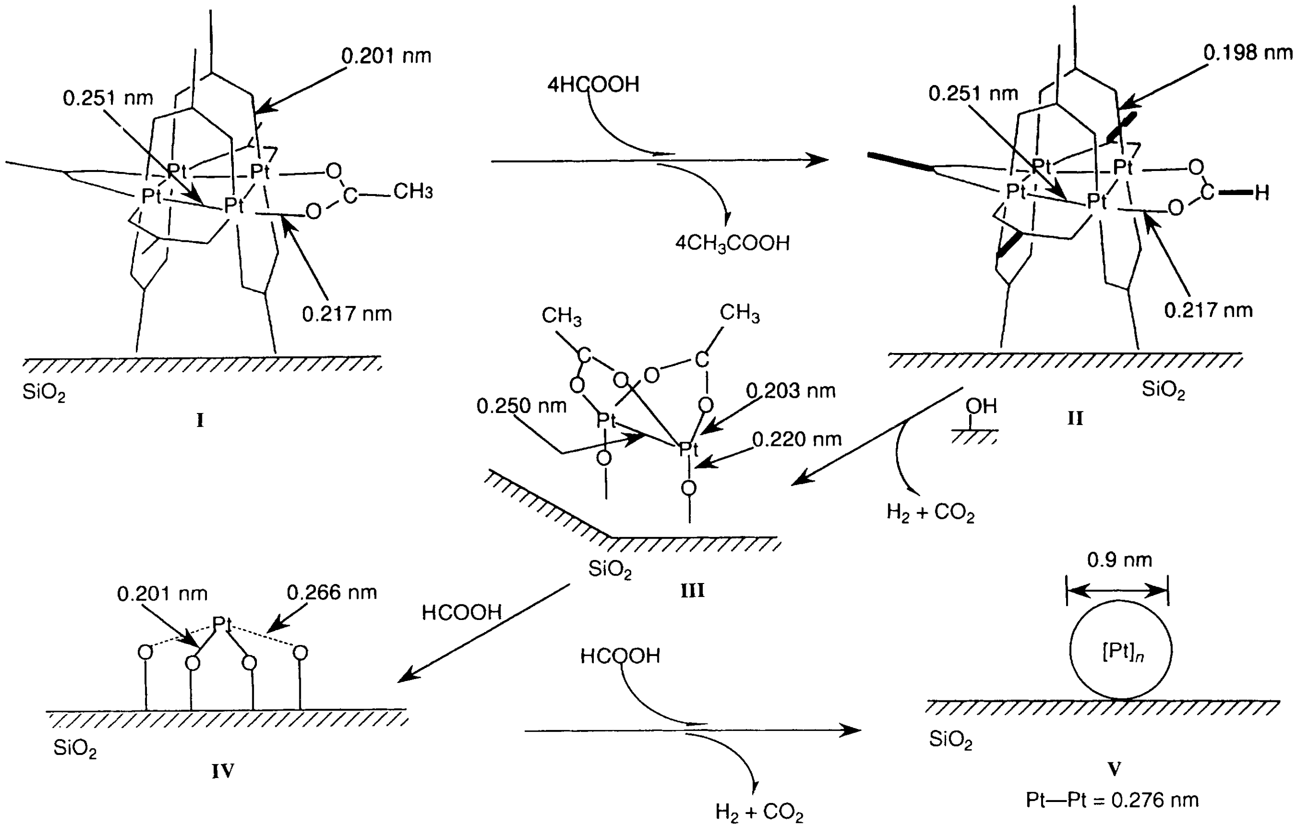

Scheme 1 Structural transformation of the $[Pt_4(\mu\text{-}CH_3COO)_8]/SiO_2$ catalyst during the course of the HCOOH decomposition reaction

When the $[Pt_4(\mu\text{-}CH_3COO)_8]/SiO_2$ sample was reduced with H_2 at room temperature, particles did not aggregate. It implies that formic acid induced the aggregation of Pt atoms, which was not enforced by H_2 formed in the formic acid decomposition. Many studies for aggregation of dispersion of metal particles by CO have been reported.[47–52] The present observation suggests the existence of mobile Pt-formates on SiO_2.

Conclusion

The catalyst employing $[Pt_4(\mu\text{-}CH_3COO)_8]$ as a precursor showed the characteristic reaction profile in the decomposition reaction of formic acid. The $[Pt_4(\mu\text{-}CH_3COO)_8]/SiO_2$ catalyst showed remarkably high catalytic activity (more than two orders of magnitude) as compared with the ion-exchanged Pt/SiO_2 catalyst. The products detected were only CO_2 and H_2 (100% dehydrogenation), while the ion-exchanged catalyst also yielded CO and H_2O in addition to CO_2 and H_2. The reaction on the cluster catalyst involved four characteristic steps: an induction period; a slow reaction period; a catalytic high-rate reaction period; and a deactivation step. There was no change in the cluster structure in the induction period, but fast replacement of the in-plane acetate ligands by formic acid took place. In the subsequent step the in-plane formate ligands decomposed to form CO_2 and H_2, and the tetramer framework reformed to give a new Pt dimer with two acetate ligands. The dimer structure was stable under vacuum, but it was transformed quickly to a catalytically active structure in excess formic acid. The EXAFS analysis revealed that the active species was Pt monomer which has both short and long Pt—O bonds at 0.201 and 0.266 nm. The Pt monomers were unstable under a formic acid atmosphere, so aggregated to form 0.9 nm particles in competition with the catalytic decomposition of formic acid. The Pt particles were almost inactive for the decomposition reaction under the present conditions. Thus, the Pt_4-clusters were found to behave dynamically, changing the structure during the course of the formic acid decomposition reaction.

References

1 *Tailored Metal Catalysts*, ed. Y. Iwasawa, D. Reidel Publishing Company, Dordrecht, 1986.
2 Y. Iwasawa, *Adv. Catal.*, 1987, **35**, 187.
3 Y. Iwasawa, *Catal. Today*, 1993, **18**, 21.
4 R. B. Bjorklund and R. L. Burwell, *J. Colloid Interface Sci.*, 1979, **70**, 383; R. L. Burwell and A. Brenner, *J. Mol. Catal.*, 1975/76, **1**, 77.
5 Y. I. Yermakov, B. N. Kuznetsov and V. A. Zakharov, *Catalysis by Supported Complexes*, Elsevier, Amsterdam, 1981.
6 W. M. H. Sachtler and J. Fahrenfort, *Proc. 2nd Int. Congr. Catal., Paris*, Editions Technip, 1961, 831.
7 P. Maes, J. J. F. Scholten and P. Zwietering, *Adv. Catal.*, 1963, **14**, 35.
8 J. M. Trillo, G. Munuera and J. N. Craido, *Catal. Rev.*, 1972, **7**, 51.
9 *Contact Catalysis*, ed. Z. G. Szabó, Elsevier, Amsterdam, 1976.
10 R. J. Madix, *Surf. Sci.*, 1979, **89**, 540.
11 F. Solymosi, J. Kiss and I. Kovács, *J. Phys. Chem.*, 1988, **92**, 796.
12 Z. G. Szabó, F. Solymosi and I. Z. Batta, *Phys. Chem., NF*, 1958, **17**, 125.
13 Z. G. Szabó, F. Solymosi and I. Z. Batta, *Phys. Chem., NF*, 1960, **23**, 56.
14 Z. G. Szabó and F. Solymosi, *Proc. 2nd Int. Congr. Catal., Paris*, Editions Technip, 1961, 1627.
15 F. Solymosi, *Catal. Rev.*, 1967, **1**, 233.
16 D. C. Grenoble, M. M. Estadt and D. F. Ollis, *J. Catal.*, 1981, **67**, 90.
17 Y. Amenomiya, *J. Catal.*, 1979, **57**, 64.
18 T. Shido, K. Asakura and Y. Iwasawa, *J. Catal.*, 1990, **122**, 55.
19 T. Shido and Y. Iwasawa, *J. Catal.*, 1991, **129**, 343.

20 T. Shido and Y. Iwasawa, *J. Catal.*, 1992, **136**, 493.
21 T. Shido and Y. Iwasawa, *J. Catal.*, 1993, **140**, 575.
22 T. Shido and Y. Iwasawa, *J. Catal.*, 1993, **141**, 71.
23 A. Deluzarche, R. Kieffer and A. Muth, *Tetrahedron Lett.*, 1977, 3357.
24 D. B. Clarke, D-K. Lee, M. J. Sandoval and A. T. Bell, *J. Catal.*, 1994, **150**, 81.
25 G. C. Chinchen, K. C. Waugh and D. A. Whan, *Appl. Catal.*, 1986, **25**, 101.
26 F. Solymosi and H. Knözinger, *J. Catal.*, 1990, **122**, 166.
27 R. G. Herman, *Stud. Surf. Sci. Catal.*, 1991, **64**, 1.
28 M. A. A. F. de C. T. Carrondo and A. C. Skapski, *J. Chem. Soc., Chem. Commun.*, 1976, 410.
29 M. A. A. F. de C. T. Carrondo and A. C. Skapski, *Acta Crystallogr., Sect. B*, 1978, **34**, 1857.
30 M. A. A. F. de C. T. Carrondo and A. C. Skapski, *Acta Crystallogr., Sect. B*, 1978, **34**, 3576.
31 A. C. Skapski and P. G. H. Troughton, *J. Chem. Soc. A*, 1969, 2772.
32 G. Albano, G. Ciani, M. I. Bruce, G. Shaw and F. G. A. Stone, *J. Organomet. Chem.*, 1972, **C99**, 42.
33 L. T. Guggenberger, *J. Chem. Soc., Chem. Commun.*, 1968, 512.
34 J. C. Calabrease, L. F. Dahl, P. Chini, G. Longoni and S. Martinengo, *J. Am. Chem. Soc.*, 1974, **96**, 2614.
35 T. Yamaguchi, Y. Sasaki, A. Nagasawa, T. Ito, N. Koga and K. Morokuma, *Inorg. Chem.*, 1989, **28**, 4311.
36 T. Yamaguchi, Y. Sasaki and T. Ito, *J. Am. Chem. Soc.*, 1990, **112**, 4038.
37 N. Kosugi and H. Kuroda, *EXAFS2*, Library of the Research Centre for Spectrochemistry, University of Tokyo, 1983.
38 T. Liu, K. Asakura, U. Lee, Y. Matsui and Y. Iwasawa, *J. Catal.*, 1992, **135**, 367.
39 F. W. H. Kampers, C. W. Engelen, J. H. C. van Hooff and D. C. Koningsberger, *J. Phys. Chem.*, 1990, **94**, 8574.
40 D. C. Koningsberger and R. P. Prins, *X-Ray Absorption*, Wiley-Interscience, New York, 1980, p. 250.
41 E. A. Stern, *Phys. Rev. B: Condens. Matter*, 1993, **48**, 9825.
42 K. Nakamoto, *Infrared and Raman Spectra of Inorganic and Coordination Compounds*, Wiley-Interscience Publication, New York, 3rd edn., 1978, p. 231.
43 S. Pinchas and I. Laulicht, *Infrared Spectra of labelled Compounds*, Academic Press, London, 1971, 126.
44 T. Yamaguchi, Y. Sasaki, A. Nagasawa, T. Ito, N. Koga and K. Morokuma, *Inorg. Chem.*, 1989, **28**, 4312.
45 D. C. Koningsberger, B. C. Gates, *Catal. Lett.*, 1992, **14**, 271.
46 R. B. Greegor and F. W. Lytle, *J. Catal.*, 1980, **63**, 476.
47 S. C. Anderson, T. Mizushima and Y. Udagawa, *J. Phys. Chem.*, 1991, **95**, 6603.
48 H. F. J. van't Blik, J. B. A. D. van Zon, T. Huizinga, J. C. D. Vism, D. C. Koningsberger and R. Prins, *J. Phys. Chem.*, 1983, **87**, 2264.
49 H. F. J. van't Blik, J. B. A. D. van Zon, T. Huizinga, J. C. D. Vism, D. C. Koningsberger and R. Prins, *J. Am Chem. Soc.*, 1985, **107**, 3139.
50 T. Mizushima, K. Tohji and Y. Udagawa, *J. Am. Chem. Soc.*, 1988, **110**, 4459.
51 T. Mizushima, K. Tohji, Y. Udagawa and A. Ueno, *J. Phys. Chem.*, 1990, **94**, 4980.
52 F. Solymosi and M. Pasztor, *J. Phys. Chem.*, 1986, **90**, 5312.

Paper 5/03308J; *Received* 23*rd May*, 1995